Co-funded by the

DISCO

Grant Agreement: 755443

DELIVERABLE D5.3

Progress on the modeling of the homogeneous $U_{0.73}Pu_{0.27}O_2$ alteration as a simulant of MOX fuel matrices in an underground disposal cell

Laurent DE WINDT & Patrick GOBLET (ARMINES, MINES ParisTech),
Valentin KERLEGUER (CEA, MINES ParisTech) & Christophe JEGOU (CEA)

Date of issue of this report: **20/05/2019**

Report number of pages: 38

Start date of project: **01/06/2017**

Duration: 48 Months

Project co-funded by the European Commission under the Euratom Research and Training Programme on Nuclear Energy within the Horizon 2020 Framework Programme		
Dissemination Level		
PU	Public	X
PP	Restricted to other programme participants (including the Commission Services)	
RE	Restricted to a group specified by the partners of the Disco project	
CO	Confidential, only for partners of the Disco project	

Table of content

1 Context and objectives

1.1 MOX vs. UOX long-term corrosion in the disposal environment

The direct disposal of irradiated fuels in deep geological repositories is a major societal issue for several countries. This option requires a thorough knowledge of the processes which may lead to any release of radionuclides into the biosphere. The French National Radioactive Waste Management Agency (Andra) has selected a Callovo-Oxfordian (COx) clay formation for the deep repository of radioactive waste. The COx reducing environment is interesting due to the low solubility of uranium dioxide (UO_2) under such conditions. UO_2 is the main constituent of the matrix of UOX (uranium oxide) spent fuels. However, the alpha activity of spent fuel may locally disrupt the reducing conditions by inducing alpha radiolysis of the surrounding water, and thus producing oxidizing species like hydrogen peroxide (H_2O_2). The transformation rate of the essentially insoluble U(IV) in the UO_2 fuel matrix to the much more soluble oxidized U(VI) compounds is a critical issue because actinides and fission products are entrapped in the UO_2 matrix. It will be responsible for the long-term radionuclide releases beyond the instant release fraction (IRF). This sequence of mechanisms is known as the radiolytic dissolution of UO_2 (Shoesmith, 2000; Ewing, 2015).

MOX (mixed plutonium and uranium oxide) fuels are currently used in several European nuclear reactors. In the hypothesis of direct disposal of spent fuel, whether the knowledge acquired for UOX fuels (Ewing, 2015) can be transferred to MOX fuels is still a debated issue. The activity of the MOX could be higher but the resistance of Pu-enriched agglomerates specifically found in MOX fuels is expected to play a beneficial role (Odorowski et al., 2016). Their results indicated a very fast dissolution of the UO_2 grains, likely due to the high alpha-activity induced by the surrounding plutonium agglomerates. On the contrary, the plutonium agglomerates were not altered over the leaching. It is consistent with the stabilizing effect of the plutonium on the oxidation of the fluorite matrix (Jegou et al., 2010b). Bauhn et al. (2018) also concluded that plutonium led to a higher stability of the fluorite structure in high-Pu content heterogeneous MOX (24%). From a scientific perspective, the understanding of the properties of Pu-enriched agglomerates can be addressed by studying simpler homogeneous MOX materials with a consistent set of leaching experiments.

In recent years, there has been an increasing focus on ensuring that data and models are capable of supporting the long-term performance assessment of geological repositories (De Windt and Spycher, 2019). This means that spent nuclear fuel experiments must be done under repository-like conditions and using materials representative of those expected in the repository. In this context, it is well known that the presence of redox active species like hydrogen in the environmental water may scavenge the radiolytic dissolution od spent-fuel (e.g. Spahiu et al., 2004; Ewing, 2015). Whether iron may also counteract the water radiolysis effects has been studied more recently (Amme et al., 2012; Liu et al., 2016; Odorowski et al., 2017). In particular, there is a need to understand the behavior of the fuel in truly reducing

conditions imposed by the corrosion of the metallic iron containers encapsulating the waste. In this context, recent laboratory experiments (Odorowski et al., 2017) investigate the effect of ferrous iron (Fe^{2+}), a reducing aqueous species coming from the corrosion of the steel canisters, on the oxidative dissolution of UO_2. The studies showed that the consumption of H_2O_2 by Fe(II) at the uranium fuel pellet's surface prevented UO_2 dissolution by H_2O_2 and leading to Fe(III)-(oxy)hydroxide precipitation on the UO_2 surface.

1.2 Chemical and reactive transport modeling for the performance assessment

Reactive transport models (RTMs), by definition, can simulate the transport and chemical reactions of multiple solutes (and gases) and their chemical interaction with rocks over various time and spatial scales. Reactive transport models have, therefore, become an invaluable component in assessing the potential performance of a repository, which requires an understanding how the various barriers evolve through space and time (De Windt and Spycher, 2019). Reactive transport modeling is also capable of great generality and flexibility and can be applied to a wide range of natural processes, as well as to engineering issues such as metal corrosion or bentonite alteration. Although the use of RTMs for deterministic predictive simulations is limited, these models can help constrain future repository behavior with sensitivity analyses and scenario modeling of the various disposal subsystems.

Data gathered from experiments (DISCO and others) are considered and used to develop thermodynamic and kinetic chemical models, as well as reactive transport model, which will provide the basis for understanding the behavior of spent nuclear fuel in the presence of components of the near field of the disposal cell. A reactive transport model has already been applied to the set of laboratory experiments of Odorowski et al. (2017). Modeling accurately reproduced the mineralogy of the system under study and predicted the nature of the phases under observation, as well as the location of their precipitation. Inverse modeling also quantified the reaction kinetics and diffusion fluxes between the different oxidizing and reducing species. Modeling showed that a lower reaction rate would displace the Fe^{2+}/H_2O_2 redox front farther away from the pellet's surface, coinciding with the release of uranium and the formation of FeOOH colloids. However, this alternative model result disagreed with the experimental data. The knowledge gained from such modeling at laboratory scales can then serve as a basis for simulations at larger scales in the context of long-term performance assessment – such as assessing whether the steel of the waste canisters inhibits the oxidative dissolution of the UO_2 spent fuel pellets.

1.3 Objectives and content of this progress report

The work package WP5 of the DISCO project is devoted to the development and application of chemical and reactive transport models describing the solid and aqueous phases of different types of spent fuels. For the present sub-task of WP5, homogeneous MOX pellets (24 wt.% Pu, $U_{0.73}Pu_{0.27}O_2$) were considered to better investigate the effect of plutonium (content and repartition) on the dissolution resistance and mechanisms. To the best of our knowledge, no data were found in the literature on the kinetics of dissolution of homogeneous $U_{1-x}Pu_xO_2$ with

high plutonium content under environmental conditions (neutral pH...). This is a key point required for the safety assessment of future disposals of any kind of MOx fuels. More generally, data is also needed for a better understanding of the chemistry of Pu-U oxide solid solutions in contact with water.

The CHESS code (chemical modeling, Section 2) and HYTEC code (reactive transport modeling, Section 2) were used with the modeling parameters directly derived from lab leaching experiments.

Modeling was first applied (in Section 3) to experiments that were conducted in carbonate water to quantify the dissolution rates of the homogeneous MOX matrix, with an emphasis on the strong disproportionation of H_2O_2 at the surface of the Pu-enriched oxide. The experimental data and kinetic parameters (Kerleguer et al.) had not been acquired in the framework of the DISCO Project. However, further modeling of the experiments were done in the DISCO Project for the sake of developing a full reactive transport model of the WP4 experiment (see below) and its application for performance assessment of the spent MOX fuel package in a disposal cell.

In a second step (Section 4), the reactive transport modeling dealt with leaching experiments that were carried out in order to determine the effect of the near-field repository environment; that is to say synthetic COx clay water with a coupon (foil) of metallic iron. This approach resulted from a tight collaboration between the experimental contribution (WP4) and modeling (WP5) on the dissolution of a homogenous $U_{1-x}Pu_xO_2$ within the DISCO project. The WP4 experiment is still in progress. Therefore, the modeling was only based on the data already available and will be improved in the final report. Again, emphasis was given on the development of a model useful for performance analysis of representative configuration of spent MOX fuel package in a disposal cell (perspectives in Section 5).

2 Modeling codes and database

2.1 Chemical modeling with CHESS

CHESS is the geochemical module of HYTEC (van der Lee et al., 2003) that simulates the chemical equilibrium state of complex aqueous systems, including minerals, organics, colloids and gases. Aqueous speciation and reaction, precipitation/dissolution of solid phases, adsorption (surface complexation, ion exchange) and reaction path simulations can be done with CHESS. The aqueous chemistry includes acid/base reactions, oxidation and reduction (redox) processes and aqueous complexation by organic and inorganic ligands. CHESS uses a mixed kinetic-thermodynamic equilibrium approach. The thermodynamic equilibrium state of the chemical system is calculated according to the usual mass action equation

$$n_a\mathrm{A} + n_b\mathrm{B} \rightleftharpoons n_c\mathrm{C} + n_d\mathrm{D} \tag{2-1a}$$

$$K = \frac{(\mathrm{C})^{n_c}(\mathrm{D})^{n_d}}{(\mathrm{A})^{n_a}(\mathrm{B})^{n_b}} = \exp\left(\frac{-\Delta_r G^0}{RT}\right) \tag{2-1b}$$

where n_i is the stoichiometric coefficient, K is the thermodynamic equilibrium constant of formation, G_0 is the Gibbs free energy of the reaction, R is the perfect gas constant and T is the absolute temperature. CHESS uses equilibrium constants, not Gibbs free energy data.

The following time-dependent kinetic rate formulation for the dissolution and precipitation of a given mineral M_i (Lasaga, 1981) is implemented in HYTEC:

$$\frac{\mathrm{d}[\mathrm{M}]}{\mathrm{d}t} = k\mathcal{A}_v \prod_i (\mathrm{A}_i)^{a_i}\left(\left(\frac{Q}{K_s}\right)^p - 1\right) \tag{2-2}$$

where the brackets stand for the concentration of the mineral M, k_i denotes the intrinsic rate constant far from equilibrium, A_v is the mineral surface area usually derived from the specific surface of the mineral, (A_j) is the activity of a given dissolved species j, a_i and p are power-constants, mechanistically-based or fitted to experimental data (a positive power stands for a catalyzing effect, a negative power for an inhibiting effect). The term $\left(\frac{Q_i}{K_s} - 1\right)$ is the saturation state dependent term, where Q_i stands for the ion activity product and K_i is the thermodynamic formation constant. If this term is greater than one (oversaturation state), Eq. 2-2 corresponds to a precipitation reaction. If this term is smaller than one (undersaturation state), Eq. 2-2 corresponds to a dissolution reaction. At equilibrium, this term becomes zero likewise the kinetic rate.

2.2 Thermodynamic data

The thermodynamic database “ThermoChimie” (Giffaut et al., 2014) was used for all the simulations. ThermoChimie developments focus on evaluating specific conditions of the near

field of radioactive waste, and the database is up-to-date with respect to the NEA compilation on the thermodynamics of fission products and actinides (Guillaumont et al., 2003).

With respect to the aqueous species, molecular hydrogen H_2(aq) produced by the anoxic corrosion of iron was fully decoupled (kinetic inhibition) from the redox reactions in the modeling, e.g. it could not reduce H_2O_2 or U(VI) in solution. The disproportionation of H_2O_2(aq) into H_2O and O_2(aq) was under kinetic control only. A sensitivity analysis were also done on the very strong aqueous ternary complexes $CaUO_2(CO_3)_3^{2-}$ and $Ca_2UO_2(CO_3)_3$(aq), including them or not in the modeling.

With respect to the solid phases, based on the literature review (Haschke and Oversby, 2002; Altmaier et al., 2013), a subset of uranium and plutonium solids that could precipitate as secondary phases was taken from the ThermoChimie database or from the literature. For the present progress report, one had:

- Uranium, UO_2:$2H_2O$(am), $UO_{2.25}$(s), $UO_{2.34}$(beta), $UO_{2.67}$(s), rutherfordine, schoepite, soddyite, studtite, uranophane;
- Plutonium, $PuCO_3OH$(s), PuO_2(coll-hyd), $Pu(OH)_4$(am), $PuO_2(OH)$(s), $PuO_2(OH)_2$:H_2O(s), $PuO_2(CO_3)$(s).

The well-crystallized UO_2, PuO_2 and $Pu(OH)_3$ were discarded since they were not expected to precipitate in the present experimental conditions. The thermodynamic constant of studtite was taken from Gimenez et al. (2014). The lower limit of the amorphous UO_2:$2H_2O$ solubility was considered in the modeling (see Odorowski et al., 2017). The selection of the secondary minerals could vary according to the experiments (i.e. Sec 3 or Sec 4). Eventually, the formation constant of $U_{0.73}Pu_{0.27}O_2$ was roughly estimated from an ideal solid solution between UO_2 and PuO_2. However, this phase was only under kinetic control in the modeling.

The anoxic corrosion of metallic iron Fe(0) was under kinetic control only. Goethite (Fe(III)-OOH) and siderite (Fe(II)CO_3) were the two secondary phases (i.e. the corrosion products) that could precipitate at thermodynamic equilibrium in the modeling.

2.3 Modeling of reactive diffusive transport with HYTEC

The diffusive transport of a reactive species *i* is coupled to chemistry in HYTEC (van der Lee et al., 2003) according to the following equation:

$$\frac{\partial \omega c_i}{\partial t} = \nabla \cdot \left(D_e(\omega) \nabla c_i \right) - \frac{\partial \omega \bar{c}_i}{\partial t} \qquad (2\text{-}3)$$

The term D_e is the effective diffusion coefficient, ω is the porosity, c_i and $\bar{c}_i$ are the mobile and immobile concentrations of a species *i* per unit volume of solution, respectively. The fixed or solid fraction is evaluated by the chemical calculations, whereas the aqueous fraction is a function of the transport processes only. From a numerical point of view, chemistry and transport are coupled through a sequential iterative algorithm. The transport module is based on the representative elementary volume (REV) approach with finite volume calculation.

In this experimental set-up without stirring, the transport of species was driven by diffusion within the solution, especially between the UO_2 pellets and the iron foil separated by some centimeters. A diffusion coefficient of 10^{-9} m^2/s in water was considered in the calculations.

3 Modeling of $U_{0.73}Pu_{0.27}O_2$ alteration under self α-radiolysis

3.1 Material and experiments

The microstructure of industrial MIMAS MOX fuels currently burned in nuclear power plants is heterogeneous with three different phases: an UO_2 matrix containing circa 3 wt.% of Pu, agglomerates with 20 wt.% of Pu, and a coating zone with an intermediate composition (Jegou et al., 2010; Odorowski et al., 2017). The modeling of a simpler MOX Fuel (24 wt.% Pu, solid solution $U_{0.73}Pu_{0.27}O_2$) with a high but homogeneous plutonium distribution is, therefore, a necessary step towards the modeling of the leaching of heterogeneous MOX matrices. This reference material is the same as the one considered in the CEA contributions to WP 4.

The unirradiated $U_{0.73}Pu_{0.27}O_2$ pellets were fabricated at CEA Cadarache (COCA Process) and stored under air in a hot-cell. After 30 years of storage period, one of the pellets was cut and then annealed under Ar/H_2 4% atmosphere to recover the radiation damage and to adjust the stoichiometry of the sample. The dimensions of the leached cut pellets were about 2 mm thick and 5.4 mm in diameter. Their density was 10.4 $kg.dm^{-3}$ (Kerleguer et al.).

The leaching experimental set-up, protocol, as well as the aqueous and solid phases had been given in Kerleguer et al. submitted paper, not performed within the DISCO project.

3.2 Modeling of uranium and plutonium aqueous chemistry

In both the experiment and the modeling, the pH of the solution was slightly alkaline and constantly buffered to 9.3 by HCO_3^- anions. The redox potential was around 0.350 V/SHE, which corresponds to mildly oxidizing conditions at this pH.

The released uranium concentrations was consistent with the uranium solubility diagram of Fig. 3-1a, where uranium is stabilized in solution as the strong U(VI) complex $UO_2(CO_3)_3^{4-}$, in the range 10^{-6} – 10^{-4} $mol.L^{-1}$ (at pH 9 and Eh around 0.35 – 0.40 V), well below the schoepite solubility limit.

The release of plutonium in solution was several orders of magnitude lower than uranium release during the whole experiment. The plutonium release was very low with a chemistry dominated by Pu(IV). The plutonium concentration in solution was almost constant, about 10^{-9} $mol.L^{-1}$. This concentration was compatible with a thermodynamic control by a amorphous $Pu(OH)_4$ phase at pH 9 and Eh around 0.35 – 0.40 V, the predominant species in solution being a carbonate complex $Pu(CO_3)_2(OH)_2^{2-}$, as shown by the solubility diagram of plutonium (Fig. 3-1b).

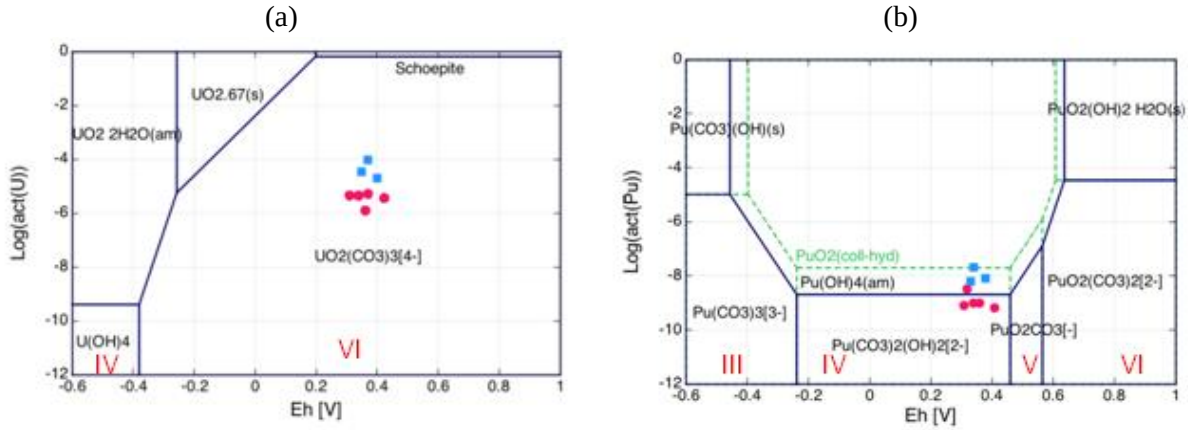

Figure 3-1. *CHESS solubility diagrams of uranium (a) and plutonium (b) as a function of redox potential (V/SHE). The diagrams were plotted at a temperature of 25 °C, a pH of 9, an activity of* HCO_3^- *of* 10^{-2}*. The red dots represent the experimental concentrations for the homogeneous MOX (Kerleguer et al.), and the blue squares the heterogeneous MOX (Odorowski et al., 2016).*

3.3 Model of kinetic processes

Under alpha irradiation, the most important species to be considered regarding $U_{0.73}Pu_{0.27}O_2$ dissolution is H_2O_2. Under alpha irradiation, the most important species to be considered regarding the dissolution of $U_{0.73}Pu_{0.27}O_2$ is H_2O_2. Several experimental studied have calibrated the oxidative dissolution of UO_2 matrices with H_2O_2. The main oxidative species in terms of concentrations is H_2O_2 according to CHEMSIMUL calculation. It is not sure that CHEMSIMUL has the full set of kinetic rate constants for all the radicals induced by radiolysis in the complex chemistry of the COx water at neutral pH. All these reactions are very sensitive to the chemistry and taking a semi-empirical calibration versus experiments where H_2O_2 is measured seems a reasonable approach within DISCO.

The hydrogen peroxide concentration in solution is controlled by one production term due to water radiolysis and two consumption terms related to disproportionation and MOX oxidation. The first step in the model development was, therefore, to take into account the kinetics of the following processes:

- H_2O_2 production by water radiolysis;
- H_2O_2 consumption by the radiolytic dissolution of the $U_{0.73}Pu_{0.27}O_2$ matrix;
- H_2O_2 disproportionation onto the surface of the $U_{0.73}Pu_{0.27}O_2$ pellet.

Two additional possible mechanisms of consumption had been discarded by Kerleguer et al. A blank experiment of hydrogen peroxide disproportionation in pure water inside the TiO_2 cell used for the experiments had shown that this process was very slow (< 1% per day). Raman spectroscopy did not indicate any precipitation of peroxide compounds at the surface of the pellets.

3.3.1 Modeling of the radiolytic production of H_2O_2

The αβγ activities of the MOX fuel were recalculated at the date of the leaching experiment and the alpha, beta and gamma dose rates determined at the surface of a pellet and in the homogeneous aqueous solution. These calculations indicated that the α irradiation field was the main source of H_2O_2 radiolytic production. The hydrogen peroxide production rate law by water radiolysis at the vicinity of the MOX pellet was

$$\frac{d[H_2O_2(aq)]}{dt} = \left(k^{prod}\right) A_v \qquad (3\text{-}1)$$

where A_v is the volumetric surface area of the pellet in $m^2.L^{-1}$. The constant k^{prod} normalized to the surface pellet was calculated to be 1.10×10^{-8} $mol.m^2.s^{-1}$ considering

- the alpha dose rate of 9730 $Gy.h^{-1}$;
- an alpha primary yield of 0.98 molecule/100eV for H_2O_2 (Kerleguer et al.);
- an average α particle range of 40 µm in water;
- the geometric surface of the pellets.

The hydrogen peroxide production rate was assumed to be constant during all the experiment.

3.3.2 Modeling of the radiolytic oxidation of $U_{0.73}Pu_{0.27}O_2$ by H_2O_2

In carbonate water, strong uranyl carbonate complexes prevent the precipitation of secondary species and uranium can be used as a tracer of the alteration (Stroes-Gascoyne et al., 2005). The dissolution of U(VI) phases can be considered relatively instantaneous. The uranium oxidation of the MOX surface by hydrogen peroxide is therefore directly linked to the uranium release rate and can be used to determine the H_2O_2 consumption rate by the uranium oxidation in the MOX. Furthermore, one mole of uranyl in solution corresponds to one mole of H_2O_2 consumption, thus the kinetic of uranium dissolution is equal to the H_2O_2 consumption. The oxidative dissolution rate law of the $U_{0.73}Pu_{0.27}O_2$ matrix was

$$\frac{d[U_{0.73}Pu_{0.27}O_2]}{dt} = \left(-k^{oxid}\ [H_2O_2(aq)]\right) A_v \qquad (3\text{-}2)$$

where A_v is again the volumetric surface area of the pellet in $m^2.L^{-1}$. This equation is rather similar to the dissolution law given by Merino et al. (2005) for the radiolytic dissolution of UO_2 powder.

Two successive dissolution regimes were observed in the experiments (Kerleguer et al.): an initial dissolution at a uranium release rate $k^{oxid}\times[H_2O_2(aq)]$ of 1.4×10^{-9} $mol.m^2.s^{-1}$ during the first 30 days, and then, a long-term dissolution regime at a rate of 8.8×10^{-11} $mol.m^2.s^{-1}$. Considering the maximal steady-state H_2O_2 concentration of 10^{-7} $mol.L^{-1}$, the corresponding rate constants k^{oxid} were about 1.4×10^{-2} $mol.m^2.s^{-1}$ and 8.8×10^{-4} $mol.m^2.s^{-1}$, respectively.

The oxidative dissolution by dissolved molecular oxygen generated by disproportionation of hydrogen peroxide was not taken into account in the modeling for the sake of simplicity, since the kinetics of the reaction of UO_2 with O_2 is known to be slower than the reaction with H_2O_2.

The decrease in the rate was probably linked to the formation of a Pu-enriched layer at the surface of the pellets. SEM-EDX analysis of Kerleguer et al. indicated a plutonium enrichment of the surface, with a homogeneous plutonium content (Pu/(U+Pu)) of 39 wt.% (against 27 wt.%, initially). The present chemical model considered a congruent dissolution with a surface precipitation/enrichment of amorphous $Pu(OH)_4$ layer. Such a passivating layer is quite consistent with the observation made on other actinides, such as thorium, uranium and neptunium (Neck and Kim, 2001).

3.3.3 Modeling of H_2O_2 disproportionation onto $U_{0.73}Pu_{0.27}O_2$

The disproportionation reaction

$$H_2O_2(aq) \rightarrow H_2O + 0.5\ O_2(aq) \tag{3-3}$$

was also modeled according to a kinetic law of first-order on H_2O_2

$$\frac{d[H_2O_2(aq)]}{dt} = \left(-\ k^{disprop}\ [H_2O_2(aq)]\right) A_v \tag{3-4}$$

where A_v is also the same volumetric surface area of the MOx pellet in $m^2.L^{-1}$.

The disproportionation rate constant $k^{disprop}$ was estimated to be 9.63×10^{-2} $L.m^{-2}.s^{-1}$ and 1.09×10^{-1} $L.m^{-2}.s^{-1}$ for the initial regime and after 30 days, respectively. It is worth noting that H_2O_2 disproportionation at long-term could, therefore, represent 99% of the H_2O_2 consumption for the homogeneous MOX pellet, against about 86% for Pu-doped UO_2 pellets (Nilson et al., 2011; Pehrman et al., 2012).

3.4 Full CHESS modeling

Figure 3-2 shows the CHESS modeling results by introducing the kinetic laws introduced above at long-term range. In the model, the amorphous $Pu(OH)_4$(am) phase was allowed to precipitate and the uranium concentration measured after 30 days was added to the calculated ones. The overall consistency of the kinetic rate constants obtained for the long-term leaching is clearly shown. The model is relatively robust for performance assessment.

Figure 3-3 shows the CHESS modeling results over the full duration of the experiment. The model took into account a negative feedback (partial passivation) of the formation of the $Pu(OH)_4$ layer on the oxidative dissolution of $U_{0.73}Pu_{0.27}O_2$. This worked well. The agreement with the experimental results was also very good over time, with the capability to simulate the smooth transition between the two regimes of uranium release. However, the passivation was modeled with a phenomenological (empirical) law

$$\frac{d[U_{0.73}Pu_{0.27}O_2]}{dt} = \left(-\ k^{oxid,pass}\ \left(\frac{1}{\kappa^n + [Pu(OH)_4]^n}\right)[H_2O_2(aq)]\right) A_v \tag{3-5}$$

inversely dependent on the layer thickness, as expected, κ is a thickness threshold around which the kinetics decreases (similar to the half-life of the Monod equation) and n stands for the roughness of the transition (the higher n is, the faster the transition is). However, this model is still strictly empirical and cannot estimate a priori the thickness threshold.

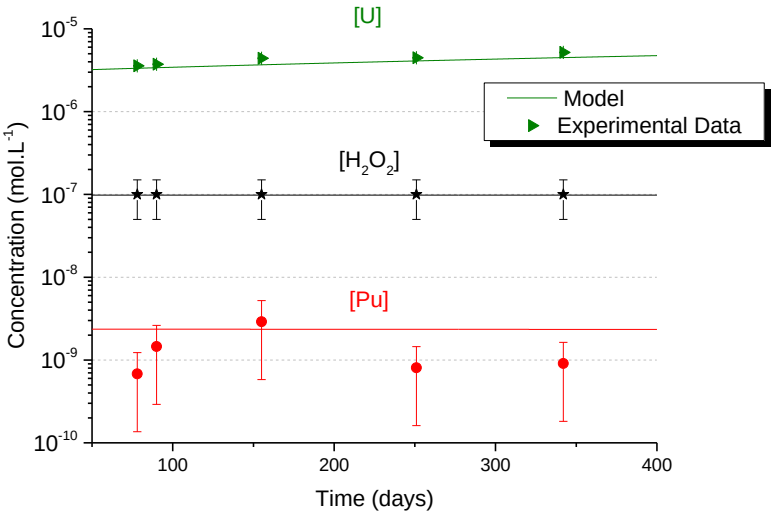

Figure 3-2. *CHESS modeling of the long-term kinetic leaching of the homogeneous MOX pellet in carbonate water (10^{-2} mol.L^{-1}).*

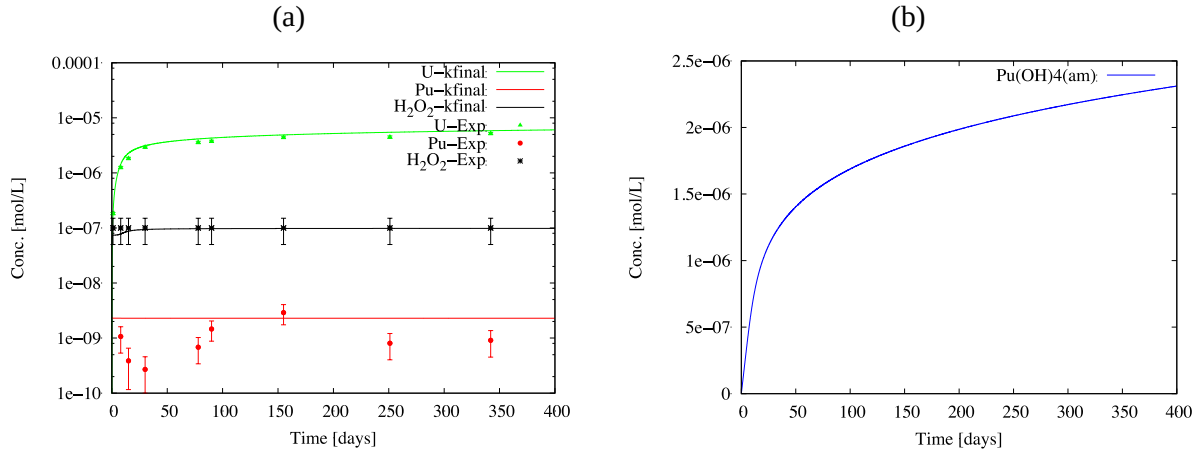

Figure 3-3. *(a) CHESS modeling of the kinetic leaching of the homogeneous MOX pellet in carbonate water (10^{-2} mol.L^{-1}) during the full experiment, from the initial state towards the long-term steady state. (b). The model takes into account a negative feedback of the formation of the Pu(OH)4 layer on the oxidative dissolution of $U_{0.73}Pu_{0.27}O_2$.*

4 Modeling of $U_{0.73}Pu_{0.27}O_2$ alteration in synthetic clay water and the presence of metallic iron

4.1 Materials and experimental set-up

The CEA-WP4 lab experiment mimics the MOX corrosion due to a possible intrusion of pore water from the Callovo-Oxfordian (COx) host rock after the corrosion and breakdown of the steel canister. A synthetic COx groundwater simulates the background groundwater chemistry and a metallic iron foil simulates the steel canister chemical reactivity. This experiment is still in progress. In particular, the aqueous leachates have been analyzed over about one hundred of days only and there is no information available on the secondary solid phases yet.

The same unirradiated $U_{0.73}PuO_{.27}O_2$ cut pellets presented in Sec 3 were introduced in an identical leaching cell at room temperature after a similar sequence of pre-leaching treatment. The atmosphere inside the glove box was argon (O_2 < 1 ppm) in order to ensure anoxic conditions. The leaching solution was a synthetic groundwater representative of Callovo-Oxfordian groundwater. Its composition is given in table 4-1, and the pH was around 7.0.

Table 4-1. *Expected composition of the synthetic Callovian-Oxfordian groundwater at 25°C.*

	$[Na^+]$	$[K^+]$	$[Ca^{2+}]$	$[Mg^{2+}]$	$[Sr^{2+}]$	$[Cl^-]$	$[SO_4^{2-}]$	$[HCO_3^-]$	[Si]
$mg.L^{-1}$	993	39.1	341	131	17.5	1454	1412	146	5.62
$mol.L^{-1}$	0.0432	0.0010	0.0085	0.0054	0.0002	0.0410	0.0147	0.0024	0.0002

Rolled 99.99% pure iron foils was used. Their size was 2.5 cm by 2.5 cm for a thickness of 125 µm and a weight of around 0.64 g. They were first pre-corroded in 180 mL of synthetic COx water for around 80-90 days in the absence of the MOX pellets. This first step was intended to ensure the presence of corrosion products on the iron foil surface, to obtain a solution chemistry containing Fe^{2+} ions not initially present in the synthetic COx water, and to have reducing conditions when the MOX pellets were introduced at a later date. After the iron pre-corrosion phase, the reactor was opened to add two MOX pellets, which were placed on a support above the iron foil. The reactor was then closed again, purged with a mixture of Ar/CO_2 3000 ppm for 30 min, and returned to a pressure of 3.5 bars. Samples of the leaching solution were regularly collected over time.

CHESS and HYTEC modeling were applied to the leaching experiments. Only time-related results could be calculated with CHESS in batch mode. The geometric configuration of the experimental set-up could be modeled with HYTEC. In this experimental set-up without stirring, the transport of species was driven by diffusion within the solution, especially between the MOX pellets and the iron foil separated by just a few centimeters. A diffusion coefficient of 10^{-9} m^2/s was considered in the calculations. Figure 4-1 shows the simulation grid of the cylindrical leaching cell used for the HYTEC calculations.

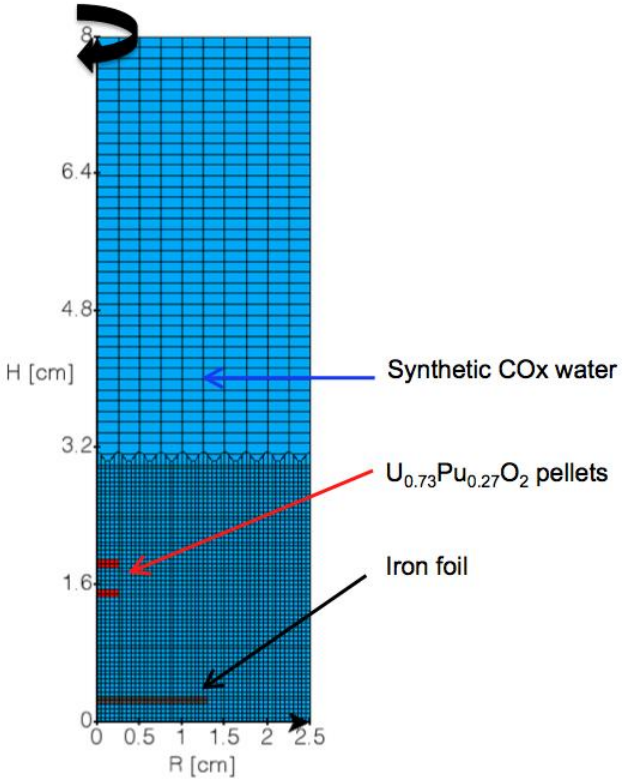

Figure 4-1. *Simulation grid of the cylindrical leaching cell used for the HYTEC calculations.*

4.2 Prerequisite on the kinetics of Fe(II)/H_2O_2 reaction in solution

The experimental and modeling study of the effect of metallic iron on the oxidative dissolution of UO_2 doped with a radioactive alpha emitter (Odorowski et al., 2017) demonstrated that the redox reaction between dissolved ferrous iron (produced by iron corrosion) and hydrogen peroxide (produced by water radiolysis and enhancing UO_2 dissolution)

$$2Fe^{2+} + H_2O_2 \rightarrow 2Fe^{3+} + 2OH^- \quad (4\text{-}1)$$

was a key reaction in the present system. The authors considered an instantaneous thermodynamic equilibrium for this homogeneous chemical reaction in solution, by lack of data but also because the experimental results were correctly modeled with this hypothesis.

To further validate this assumption a kinetic control were introduced in the model based on a literature review. Many studies dealt with the Fenton reaction under acidic to slightly acidic conditions. Only few papers relevant for Eq. 4-1 under geological conditions could be found.

The combination of two first-order reactions is commonly encountered in the literature

$$R(mol.L^{-1}.s^{-1}) = \frac{d[H_2O_2]}{dt} = \frac{1}{2}\frac{d[Fe^{2+}]}{dt} = -k\ a_{Fe^{2+}}\ a_{H_2O_2} \quad (4\text{-}2)$$

where *a* is the activity of the dissolved species, and *k* is the rate constant. The value of *k* varies over several orders of magnitude

- from 5×10^{1} mol.L^{-1}.s^{-1} in acidic pure water (CHEMSIMUL data: from Hardwick, 1956; Christensen and Bjergbakke, 1986);
- to more than 10^{4} mol.L^{-1}.s^{-1} in moderately saline and alkaline water, likewise the COx groundwater (Millero and Sotolongo, 1989).

Figure 4-2 shows the value of the rate constant *k* of Equation 4-2 with respect to the pH and the ionic strength in seawater at 25 °C (Millero and Sotolongo, 1989). The strong effect of pH is due to the higher reactivity of $Fe(OH)^{+}$ hydroxyl complex (whose proportion increases with pH) compared to pure Fe^{2+} ions. The effect of the ionic strength is much more moderate. Still in Millero and Sotolongo, 1989, a rate constant value of about 10^{5} mol.L^{-1}.s^{-1} is reported in pure 10^{-2} M $NaHCO_3$ solution at 25 °C; that is to say fully representative of the present leaching conditions.

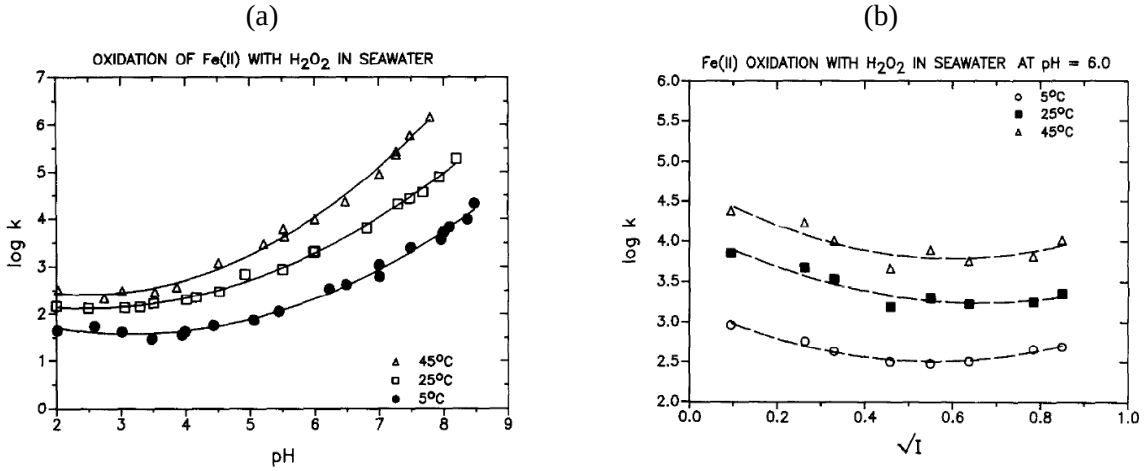

Figure 4-2. *The effect of pH (a) and the ionic strength (b) on the rate constant of the oxidation of Fe(II) with H_2O_2 in seawater at different temperatures (Millero and Sotolongo, 1989).*

Furthermore, the mass transport over space plays an important role. The hydrogen peroxide generated within the alpha-track is initially very close to the fuel surface (tens of μm), while the ferrous iron generated through corrosion of metallic iron lies usually much longer from the fuel surface (cm scale). The sensitivity analysis of these coupled processes was, therefore, performed with the reactive transport software HYTEC.

The HYTEC results of Figure 4-3a show that the calculated concentration of uranium is in good agreement with the experimental data at thermodynamic equilibrium or fast kinetics, whereas modeling with the lower kinetic rate overestimates uranium release. Fig. 4-3b indicates that iron concentration is not sensitive to kinetics in the present system, due to the relatively higher concentration of Fe(II) with respect to H_2O_2 and the solubility control by siderite.

Many studies dealt with the Fenton reaction under acidic to slightly acidic conditions, but at neutral pH Fe(III) is insoluble, precipitates, and, therefore does not participate to such a reaction.

This sensitivity analysis having proved that the kinetics was fast, the homogeneous reaction between Fe(II) and H_2O_2 was modeled at thermodynamic equilibrium for the sake of reducing computional CPU time.

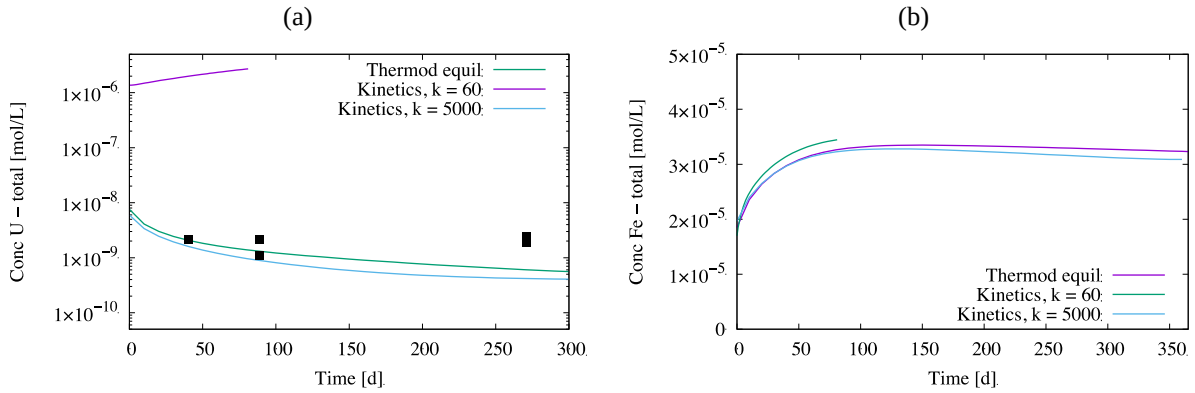

Figure 4-3. *HYTEC modeling of Pu-doped UO_2 pellets in synthetic COx groundwater in presence of a pristine iron foil: sensitivity of the calculated concentrations of dissolved uranium (a) and iron (b) with respect to kinetics, Eq. 4-2.*

4.3 The full set of kinetic laws used in the modeling

The chemical and reactive transport models considered the set of kinetics laws that had been validated on the leaching of $U_{0.73}Pu_{0.27}O_2$ in carbonate water (Sec 3). That is to say:

- the alpha-radiolytic production of H_2O_2

$$\frac{d[H_2O_2(aq)]}{dt} = \left(k^{prod}\right) A_v \qquad (4\text{-}3)$$

with k^{prod} = 1.10×10^{-8} mol.m^2.s^{-1}.

- the disproportionation of H_2O_2 on the surface pellet

$$\frac{d[H_2O_2(aq)]}{dt} = \left(-k^{disprop}\ [H_2O_2(aq)]\right) A_v \qquad (4\text{-}4)$$

with $k^{disprop}$ = 1.09×10^{-1} L.m^{-2}.s^{-1} mol.m^2.s^{-1}, plus a simplified approach in HYTEC cases where disproportionation is taken into account by dividing k^{prod} by a factor 100 (i.e. a 99% consumption of hydrogen peroxide) without considering Eq 4-3.

- the oxidative dissolution of the $U_{0.73}Pu_{0.27}O_2$ solid solution

$$\frac{d[U_{0.73}Pu_{0.27}O_2]}{dt} = \left(-k^{oxid}\ [H_2O_2(aq)]\right) A_v \qquad (4\text{-}5)$$

with k^{oxid} = 8.8×10^{-4} mol.m^2.s^{-1} (long-term kinetics, > 30 days), plus a sensitivity analysis with k^{oxid} = 1.4×10^{-2} mol.m^2.s^{-1} (initial kinetics).

In addition, the $U_{0.73}Pu_{0.27}O_2$ solid solution is also expected to dissolve under reducing conditions in lack of any oxidative species. To the best of our knowledge, there is no information in the literature about the corresponding rate constant k^{red}. As a starting point, the kinetics of Pu-doped UO_2 pellet were taken into account

$$\frac{d[U_{0.73}Pu_{0.27}O_2]}{dt} = \left(-k^{red}\right) A_v \quad (4\text{-}6)$$

A rate constant value of 2×10^{-12} mol.m^{-2}.s^{-1} was taken from the literature as in Odorowski et al. (2017). Bruno et al. (1991) gave a dissolution rate of UO_2 under reducing conditions of 1.9×10^{-12} mol.m^{-2}.s^{-1} for 7 ≤ pH ≤ 11, and Ulrich and al. (2008) gave a similar value of 2×10^{-12} mol.m^{-2}.s^{-1} for 3 ≤ pH ≤ 8. Both studies were carried out in pH ranges representative of the pH measured in our leaching experiments (pH ~ 7). This kinetics under reducing conditions is clearly slower than the oxidative dissolution one. The mass balance on the release of uranium (in solution, colloidal and sorbed) at the end of the WP4 experiment will be stopped will provide some insights into the actual value of k^{red}, in particular whether the plutonium content reduces the kinetics compared to a pure UO_2 phase.

Eventually, the corrosion of metallic iron Fe(0) in anoxic media can be written as:

$$Fe(0) + 2\,H_2O \rightarrow Fe^{2+} + 2\,OH^- + H_2 \quad (4\text{-}7)$$

A kinetic constraint was imposed on this corrosion process using the following law:

$$\frac{d[Fe(0)]}{dt} = -k^{corr}\, A_v \quad (4\text{-}8)$$

where k^{corr} is the intrinsic kinetic rate constant of iron corrosion under anoxic conditions (mol.m^{-2}.s^{-1}), A_v is the volumetric surface area of metallic iron (m^2.L^{-1}). De Combarrieu et al. (2007) found a rate of 6×10^{-9} mol.m^{-2}.s^{-1} for the dissolution of metallic iron in synthetic COx water at 90°C and in the presence of clay introduced as a powder in the reactor. This kinetic rate constant k_{anox} was lowered to 3×10^{-9} mol.m^{-2}.s^{-1} by fitting the Fe aqueous concentration in a pre-corrosion experiment of the iron foil carried out in the synthetic COx water at 25°C. This slight decrease with temperature is consistent with the low activation energy of iron corrosion, about 15 kJ.mol^{-1}.

In all cases, the secondary phases were modeled at thermodynamic equilibrium without kinetics. That is to say the corrosion products (e.g. goethite, siderite), $Pu(OH)_4$(am), UO_2:2H_2O(am), etc.

4.4 Uranium and plutonium releases and precipitation

CHESS modeling in batch mode was performed to get a first idea of the system evolution. Figure 4-4a shows that the release of uranium in the COx water/iron system became lowered by four orders of magnitude compared to carbonate water, both in the experiment and in modeling. The concentration quickly decreased close to the thermodynamic equilibrium with the amorphous U(IV) phase UO_2:$2H_2O$. This dramatic effect of the environment is very similar to what had been obtained for Pu-doped UO_2 with an alpha activity corresponding to a spent UOX of 50 years old (Fig. 4-5). Odorowski et al. (2017) showed that the COx groundwater itself decreased the uranium concentration but that iron played the main role by fully scavenging H_2O_2 reactivity and the oxidative dissolution of UO_2. The same process did occur with the present MOX fuel most probably.

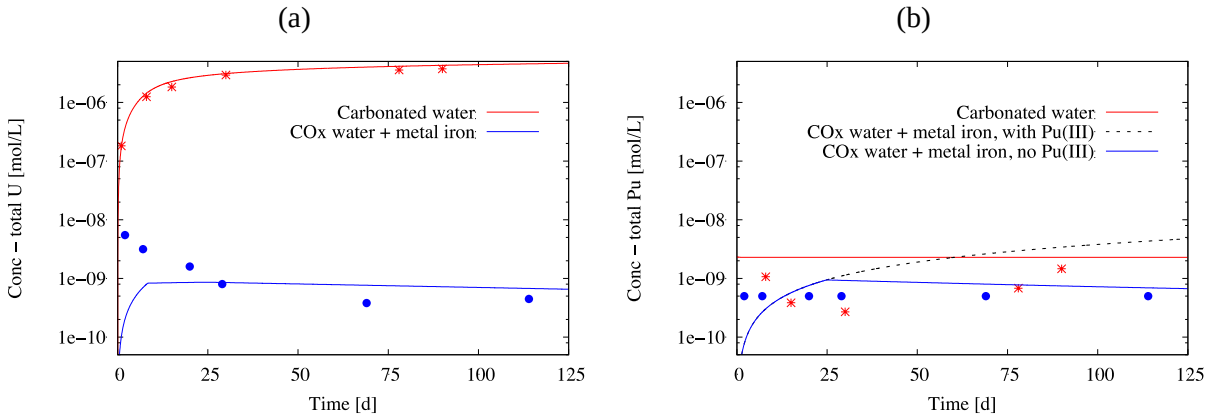

Figure 4-4. (a) *Experimental and CHESS modeling results of uranium (a) and plutonium (b) of the homogeneous MOX pellet in carbonate water and in synthetic COx groundwater in presence of a pre-corroded iron foil.*

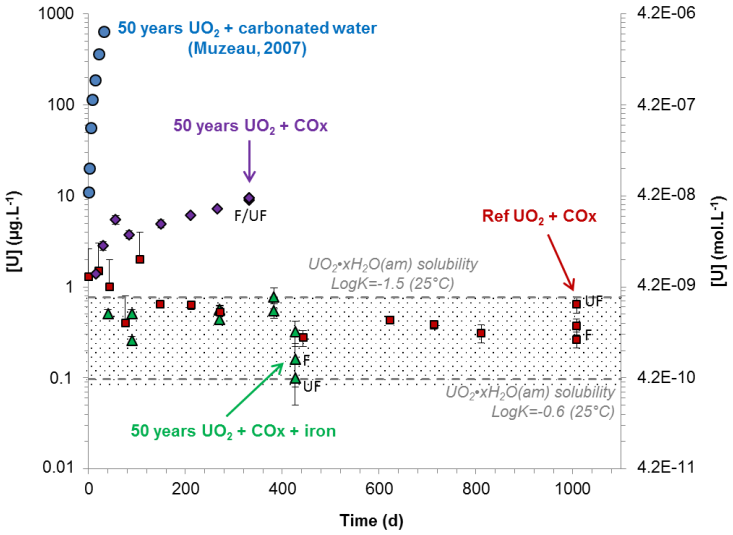

Figure 4-5. *Evolution of uranium concentrations in solution during leaching of Pu-doped UO_2 pellets (alpha activity corresponding to a 50-year UOX) in different environments (Odorowski et al, 2017).*

The release of plutonium was not well captured by the chemical model when the whole redox states of the plutonium were taken into account (Fig. 4-4b, dashed line). The Pu aqueous concentration increases constantly in time to reach levels above the experimental measured concentrations, in disagreement with the experimental data, despite the long-term (and lowest) oxidation rate of $U_{0.73}Pu_{0.27}O_2$ (Eq. 4-5, $k^{oxid} = 8.8\times10^{-4}$ mol.m^2.s^{-1}) was assumed only. In the modeling, the Pu(III) species predominate in solution over the Pu(IV) species since the redox condition were sufficiently reducing (Eh ~ -200 mV, pH ~ 7.3, Fig. 4-6) due to the presence of Fe(II) in solution, to allow the reduction of Pu(IV) into Pu(III). The measured experimental Eh value was in the range -40 mV – 120 mV. This measure was semi quantitative only. However, this proved that the system was mildly reducing and not strongly reducing (H_2 was not an active redox species).

The reducing condition of the modeling prevented a solubility control by the secondary formation of amorphous $Pu(OH)_4$. Increasing the thermodynamic stability of the Pu-enriched leached layer or, equivalently, considering a more stable phase like led to the precipitation but some Pu(III) remained in solution. Possibly, the reduction of Pu(IV) to Pu(III) by Fe(II) could be hindered within the altered layer. Fixing the redox potential Eh to 100 mV in the modeling led to the right level of plutonium concentration but then overestimated the uranium concentration. The precipitation of amorphous $Pu(OH)_3$ could be another possibility. The global mechanism is, therefore, not well understood for the moment. When the WP4 experiment will be stopped, the mass balance (in solution, colloidal and sorbed) on the release uranium and plutonium and XPS analysis will provide some insights into the chemistry of plutonium. For the moment, a pragmatic approach was to decouple the Pu(III) species from the modeling, which reproduced correctly the full set of experimental data.

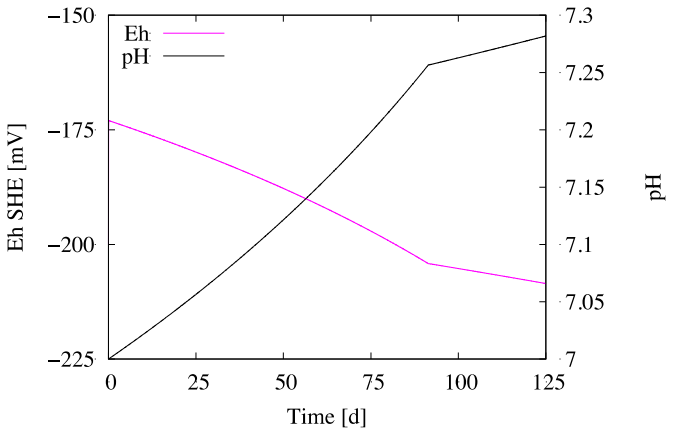

Figure 4-6*. CHESS modeling of the Eh and pH evolution related to the corrosion of the iron foil during the leaching of the homogeneous MOX in synthetic COx groundwater.*

Figure 4-7 shows the HYTEC reactive transport modeling of the leaching cell after 125 days. The dissolved of uranium and plutonium are homogenously diluted into the synthetic COx groundwater to reach concentrations identical to those of the CHESS batch modeling. The precipitation of the secondary phases UO_2:2H_2O and $Pu(OH)_4$(am) are located onto the surface pellets only. Increasing the rate constant of oxidative dissolution k^{oxid} from 8.8×10^{-4} mol.m^2.s^{-1} (base case) to 1.4×10^{-2} mol.m^2.s^{-2} (maximum value) did not change the calculated

uranium and plutonium releases, meaning that the only active process was the slow dissolution under reducing conditions.

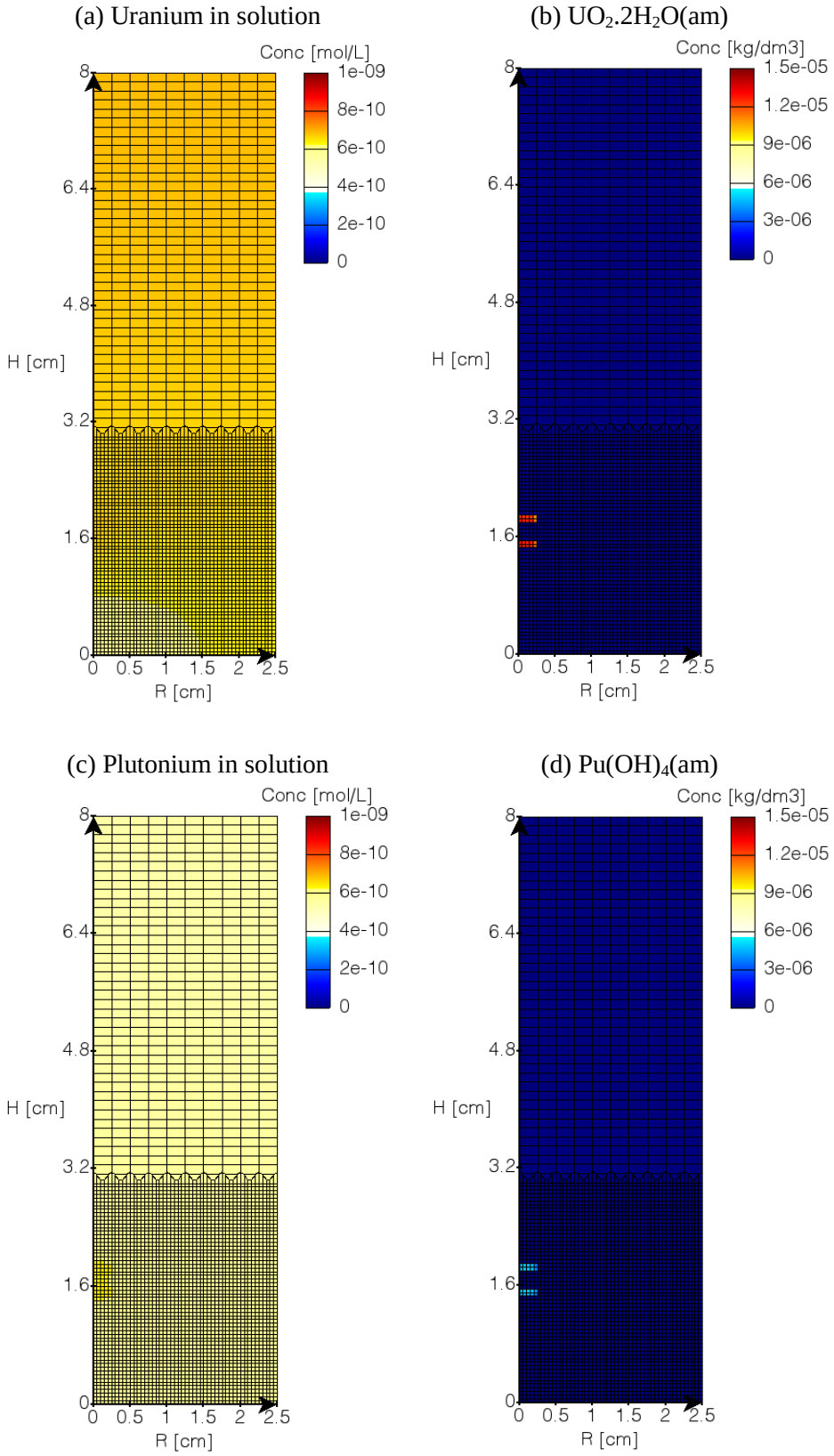

Figure 4-7. *HYTEC modeling of the aqueous concentrations of uranium (a) and plutonium (c) and the precipitation of uranium (b) and plutonium (d) phases, after 125 days of leaching of homogeneous MOX pellet in synthetic COx groundwater in presence of a pre-corroded iron foil.*

4.5 Corrosion of the iron foil

A pre-corroded state of the iron foil was assumed in all the modeling results discussed hereafter. The CHESS modeling of the dissolved concentration of iron is about 5×10^{-5} mol.L^{-1} (Fig. 4-8a) under the control by the equilibrium with the corrosion product siderite. The measured concentrations during the leaching over the first 125 days were about 1×10^{-3} mol.L^{-1}. Therefore, the present modeling underestimates Fe(II) concentration in solution by one order of magnitude. A first explanation is that siderite was taken as a proxy for the corrosion products in lack of solid analysis for the moment. Chukanovite is an alternative carbonated corrosion product (Odorowski et al., 2017) and its solubility is higher than the siderite one. As a second explanation, the corrosion products were probably not at equilibrium with the solution. This limitation of the present reactive transport model will be improved during the second half of the DISCO project.

The HYTEC modeling of the corrosion of the iron foil (Eqs. 4-6 and 4.7) releases ferrous iron ions into the synthetic COx solution (Fig. 4-9a). A fraction of them precipitates as the carbonated corrosion product siderite (Fig. 4-9c), the remaining fraction diffuses from the foil throughout the cell solution. Fig. 4-9b also shows that the pH profile was not fully homogeneous within the aqueous solution. The model predicted a slight increase in pH locally around the iron foil, because its anoxic corrosion liberates hydroxide ions (Eq. 4-6). This local increase in pH shifts the carbonate equilibriums and favors the precipitation of the carbonated minerals siderite $FeCO_3$ (Fig. 4-9c) and calcite $CaCO_3$ (Fig. 4-8d) according to the following set of reactions:

$$HCO_3^- + OH^- \rightarrow CO_3^{2-} + H_2O \quad \text{(4-9a)}$$

$$Fe^{2+} + CO_3^{2-} \rightarrow FeCO_3 \quad \text{(4-9b)}$$

$$Ca^{2+} + CO_3^{2-} \rightarrow CaCO_3 \quad \text{(4-9c)}$$

Precipitation occurred onto the surface of the iron foil. The synthetic COx groundwater was the source of calcium and bicarbonates.

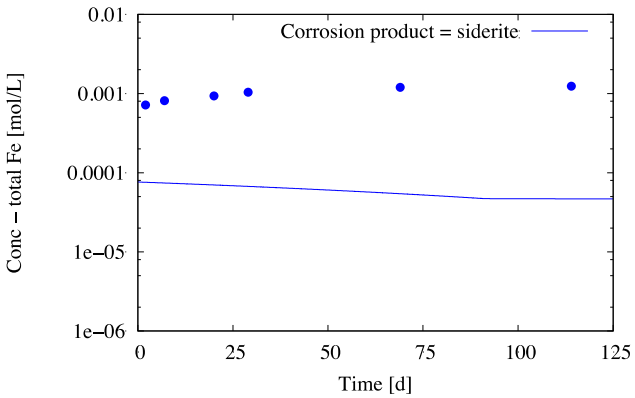

Figure 4-8. *Experimental and CHESS modeling results of ferrous iron concentration in the solution controlled by the precipitation of siderite during the leaching of homogeneous MOX pellet in synthetic COx groundwater in presence of a pre-corroded iron foil.*

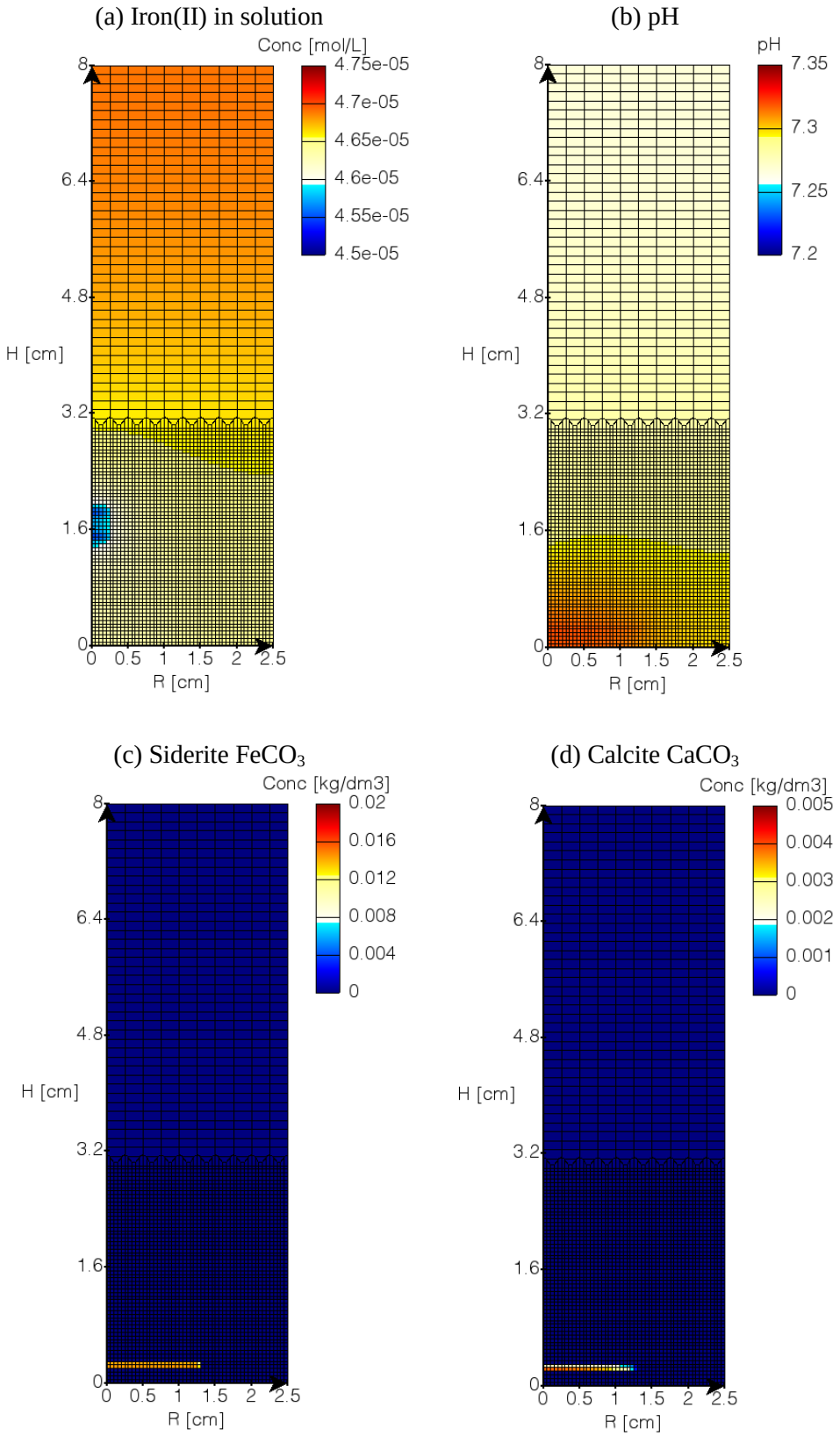

Figure 4-9. *HYTEC modeling of ferrous iron concentration (a) and pH (b) in the solution, as well as the precipitation of siderite and calcite (d) on the iron foil, after 125 days of leaching of homogeneous MOX pellet in synthetic COx groundwater in presence of a pre-corroded iron foil.*

4.6 Scavenging effect of Fe(II) versus the H_2O_2 plume

As in the CHESS modeling, HYTEC modeling gives a redox potential that is mildly reducing (Fig. 4-10a). The redox potential is mostly controlled by the dissolved aqueous release of ferrous iron by the corrosion of the iron foil (Fig. 4-10c). It is worth mentioning that the redox effect of the molecular oxygen produced by the possible disproportionation of hydrogen peroxide is not considered in the present modeling.

The complete consumption of hydrogen peroxide by aqueous ferrous iron can be schematized by the following mass balance equation

$$\frac{1}{2}H_2O_2 + Fe^{2+} \rightarrow Fe^{3+} + OH^- \qquad (4\text{-}10)$$

The fact this reaction prevents any oxidative dissolution of $U_{0.73}Pu_{0.27}O_2$ in the modeling is supported by three modeling results. First, the lack of hydrogen peroxide in solution that could raise the potential towards more oxidizing values (Fig. 4-10b). Then, the (slight) decrease of Fe(II) concentration in the solution in contact with the MOX pellets; as Fe(II) induced by iron corrosion and diffusing from the iron foil towards the MOX pellet's surface (Fig. 4-10c). Eventually, the precipitation of Fe(III)-(oxy)hydroxide goethite on the pellet surface (Fig. 4-10d) from the Fe(III) species produced by the equation 4.8; which is consistent with the precipitation of akaganeite (FeOOH) observed in the experiments of Odoroswki et al. (2017).

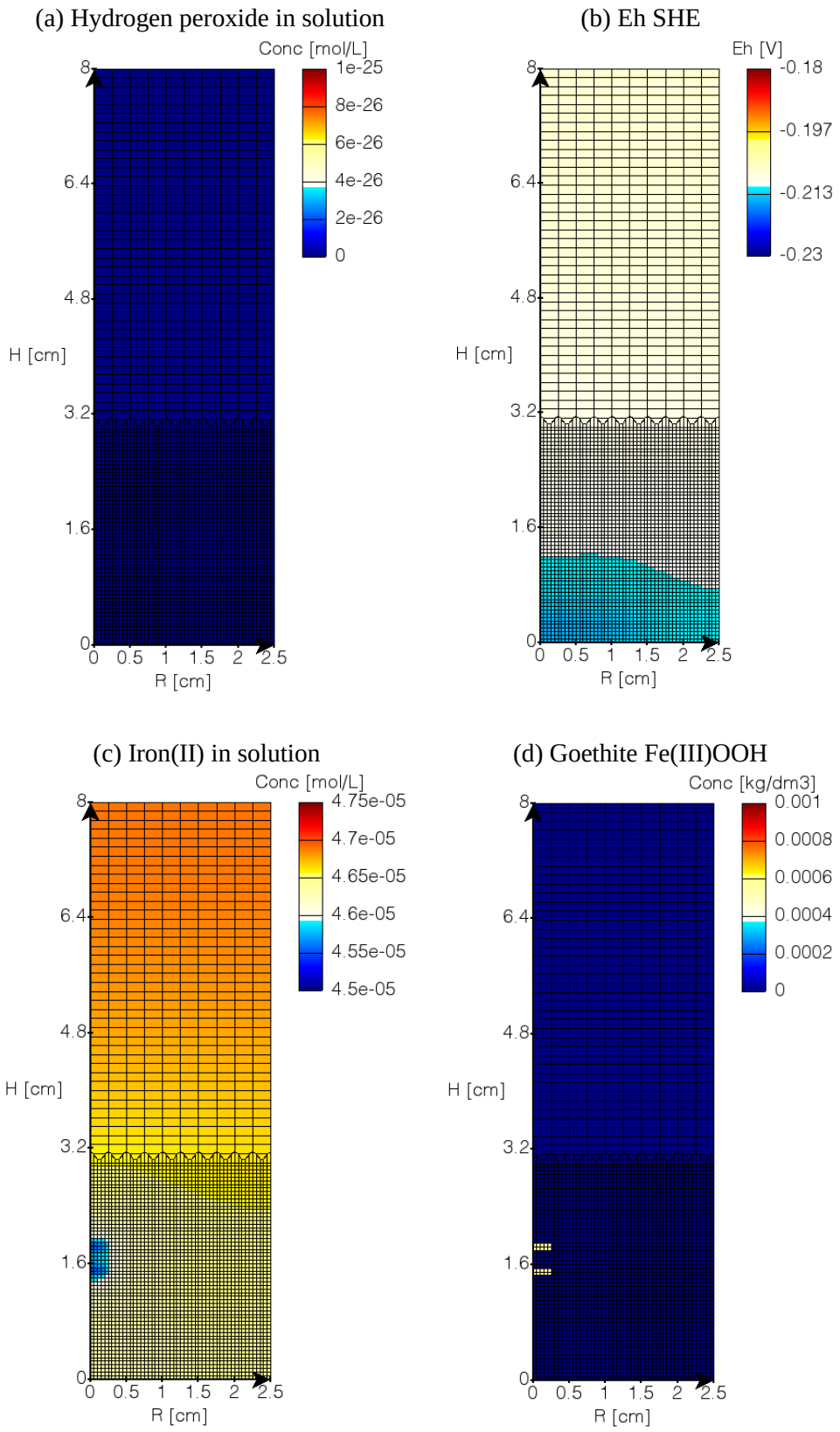

Figure 4-10. *HYTEC modeling of redox potential (a), hydrogen peroxide (b) and ferrous iron (c) concentrations in the solution, as well as the precipitation of goethite (d) on the MOX pellet, after 125 days of leaching of homogeneous MOX pellet in synthetic COx groundwater in presence of a pre-corroded iron foil.*

Figure 4-11 gives the sensitivity analysis by HYTEC modeling on the ferrous iron and hydrogen peroxide concentrations in the solution as a function of the disproportionation efficiency. The smaller the disproportionation is, the higher the H_2O_2 global stock available for corrosion is, the more iron flux is required to kill the oxidant plume. Only the worst unrealistic case of no disproportionation at all is able to keep a bubble of H_2O_2 and to attack the MOX pellet. However, this result should be confirmed when the model will correctly simulate the iron concentration in solution, which is for the moment underestimated by a factor 10. Modeling also showed that no-disproportionation case would displace the Fe^{2+}/H_2O_2 redox front farther away from the MOX pellet's surface, coinciding with the formation of FeOOH colloids; which was in disagreement with the experimental results.

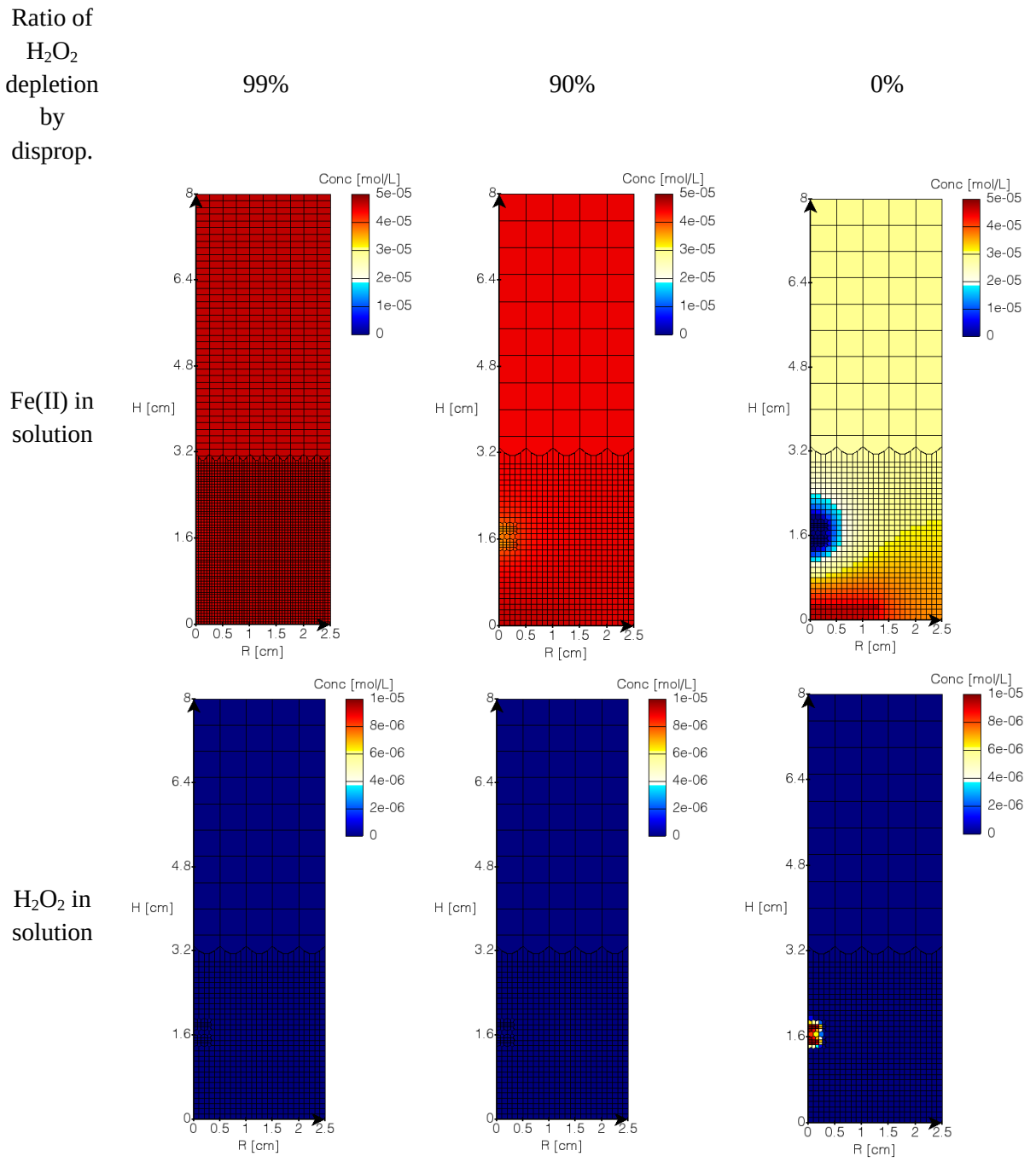

Figure 4-11. *Sensitivity analysis by HYTEC modeling on the ferrous iron and hydrogen peroxide concentrations in the solution versus the disproportionation efficiency, after 125 days of leaching of homogeneous MOX pellet in synthetic COx groundwater in presence of a pre-corroded iron foil.*

5 Intermediate conclusion and perspectives

The present study has brought insights into the two main objectives of the DISCO project: to enhance the understanding of spent fuel matrix dissolution under conditions representative of failed containers (carbon steel here) in reducing repository environments, from the one hand, to assess whether novel types of fuel (MOX here) behave like the conventional ones (UOX here) from the other hand. Both chemical and reactive transport modeling have dealt with the leaching experiments of homogenous MOX pellet, 1) first in carbonate water to get the intrinsic kinetics of dissolution (Kerleguer et al., experiments not within the DISCO Project), 2) then in synthetic COx water representative of the French disposal site groundwater in the presence of an iron foil simulating the container. The latter is the CEA-WP4 lab of the DISCO Project, experiment that mimics the possible intrusion of pore water from the host rock after the corrosion and breakdown of the steel canister. This experiment is still under progress.

The overall consistency of the kinetic rate constants (production, disproportionation, oxidative dissolution) obtained for the long-term (> 30 days) leaching of the unirradiated homogeneous $U_{0.73}Pu_{0.27}O_2$ pellet in carbonate water has been clearly shown. The release of uranium, the concentration of plutonium controlled by the precipitation of an amorphous $Pu(OH)_4$ altered layer, and the high disproportionation of hydrogen peroxide by the $U_{0.73}Pu_{0.27}O_2$ surface have been correctly modeled. A sensitivity analysis can be done in future performance calculations while considering the initial faster dissolution of the $U_{0.73}Pu_{0.27}O_2$ solid solution. In comparison with the experimental results of Odorowski et al. (2016), the plutonium content makes the solid solution more resistant than UO_2 towards leaching. Despite a higher alpha activity due to the higher plutonium content, the release of uranium from $U_{0.73}Pu_{0.27}O_2$ is lower and the consumption of hydrogen peroxide is higher. The two models, for UO_2 and $U_{0.73}Pu_{0.27}O_2$, should be now combined for a better description of heterogeneous microstructural MOX (UO_2 matrix, Pu-enriched agglomerate) currently in use in the nuclear power plants.

Both experimental and modeling results have shown that the release of uranium in groundwater in the presence of metallic iron became very significantly lowered compared to carbonate water conditions. This is very similar to what have been obtained on alpha-doped UO_2 pellet (Odorowski et al., 2017). In the modeling, iron corrosion has been identified to be a key factor because Fe(II) released in solution by the iron foil anoxic corrosion consumes H_2O_2 produced by alpha-radiolysis of water. This redox reaction occurs where radiolytic H_2O_2 is produced, i.e. on the surface of the MOX pellets. The Fe(III) produced precipitates immediately onto the MOX pellets as a Fe(III)OOH. Thanks to this consumption of H_2O_2, the oxidative dissolution is strongly inhibited by the presence of metallic iron, again despite a higher alpha activity due to the higher plutonium content. The CHESS/HYTEC model developed as part of this work led to results in agreement with the preliminary solution analysis, but should be further validated by mass balance (dissolved, colloidal and sorbed fractions for U and Pu) as well as the observation and analysis of the solid phases at the end of the leaching tests. The solubility of iron corrosion products should also be better captured by the model.

The knowledge gained from such reactive transport modeling at laboratory scales can then serve as a basis for simulations at larger scales and duration to better assess and constrain the long-term evolution of a disposal cell of spent MOX fuel. In the second half of the DISCO project, the reactive transport model will be applied to a disposal package and disposal cell developed on the basis of the present French vitrified waste concept. One single MOX assembly will be inserted in carbon steel overpack. The overpack will directly be placed in the a carbon steel liner within the COx host rock. For the sake of simplicity, the MOX complexity will be reduced to the unirridiated homogeneous solid solution; possibly extended to the heterogeneous microstructure of unirridiated heterogeneous MOX fuel. Several types of corrosion products of the steel container and, therefore, various concentration limits of dissolved Fe(II), could be considered in the modeling, i.e. corresponding to different corrosion product of steel (chukanovite, siderite, magnetite or iron-silicates as greenalite).

Acknowledgement

The research leading to these results has received funding from the European Commission Horizon 2020 Research and Training Programme of the European Atomic Energy Community (EURATOM) (H2020-NFRP-2016-2017-1) under grant agreement n° 755443 (DisCo project).

6 References

Altmaier, M., Gaona, X., Fanghänel, T. (2013). Recent Advances in Aqueous Actinide Chemistry and Thermodynamics. Chem Rev 113, 901–943.

Amme, M., Pehrman, R., Deutsch, R., Roth, O., Jonsson, M. (2012). Combined effects of Fe(II) and oxidizing radiolysis products on UO_2 and PuO_2 dissolution in a system containing solid UO_2 and PuO_2. J Nucl Mater 430, 1–5.

Bauhn, L., Hansson, N., Ekberg, C., Fors, P., Delville, R., Spahiu, K. (2018). The interaction of molecular hydrogen with α-radiolytic oxidants on a $(U,Pu)O_2$ surface. J Nucl Mater 505, 54–61.

Bruno, J., Casas, I., Puigdomenech, I. (1991). The kinetics of dissolution of UO_2 under reducing conditions and the influence of an oxidized surface-layer (UO_{2+x}) - Application of a continuous flow-through reactor. Geochim Cosmochim Acta 55, 647–658.

Christensen, H., Bjergbakke, E. (1986). Application of CHEMSIMUL for groundwater radiolysis. Nucl Chem Waste Manag 6, 265–270.

De Combarieu, G., Barboux, P., Minet, Y. (2007). Iron corrosion in Callovian-Oxfordian argilite: From experiments to thermodynamic/kinetic modelling. Phys. Chem. Earth 32, 346–358.

De Windt, L., Spycher, N. (2019). Reactive Transport Modeling: A Key Performance Assessment Tool for the Geologic Disposal of Nuclear Waste. Elements 15, 99–102.

Ewing, R. C. (2015) Long-term storage of spent nuclear fuel. Nat Mater 14, 252–257.

Giffaut, E., Grive, M., Blanc, P., Vieillard, P., Colas, E., Gailhanou, H., Gaboreau, S., Marty, N., Made, B., Duro, L. (2014). Andra thermodynamic database for performance assessment: ThermoChimie. Appl Geochem 49, 225–236.

Gimenez, J., de Pablo, J., Casas, I., Martinez-Llado, X., Rovira, M., Torrents, A. M. (2014). Solubility study and point of zero charge of studtite ($UO_2O_2{\cdot}4H_2O$). Appl Geochem 49, 42–45.

Guillaumont, R., Fanghanel, T., Neck, V., Fuger, J., Palmer, D. A., Grenthe, I., Rand, M. H. (2003). Update on the Chemical Thermodynamics of Uranium, Neptunium, Plutonium, Americium, and Technetium. Elsevier, Amsterdam, The Netherlands.

Hardwick, T.J. (1957). The rate constant of the reaction between ferrous ions and hydrogen peroxide in acid solution. Canad J Chem 35, 428–436.

Haschke, J.M., Oversby, V.M. (2002). Plutonium chemistry: a synthesis of experimental data and a quantitative model for plutonium oxide solubility. J Nucl Mater 305, 187–201.

Jégou, C., Caraballo, R., De Bonfils, J., Broudic, V., Peuget, S., Vercouter, T., Roudil, D. (2010a). Oxidizing dissolution of spent MOX47 fuel subjected to water radiolysis:

Solution chemistry and surface characterization by Raman spectroscopy. J Nucl Mater 399, 68–80.

Jégou, C., Caraballo, R., Peuget, S., Roudil, D., Desgranges, L. Magnin, M. (2010b). Raman spectroscopy characterization of actinide oxides $(U_{1-y}Pu_y)O_2$: Resistance to oxidation by the laser beam and examination of defects. J Nucl Mater 405, 235–243.

Kerleguer, V., Jégou, C., De Windt, L., Broudic, V., Jouan, G., Miro, S., Tocino, F., Martin, C. The mechanisms of alteration of a homogeneous $U_{0.73}Pu_{0.27}O_2$ MOx Fuel under alpha radiolysis, in preparation for J Nucl Mater.

Liu, N., Wu, L., Qin, Z., Shoesmith, D.W. (2016). Roles of radiolytic and externally generated H_2 in the corrosion of fractured spent nuclear fuel. Environ. Sci. Technol. 50, 12348–12355.

Merino, J., Cera, E., Bruno, J., Quinones, J., Casas, I., Clarens, F., Gimenez, J., de Pablo, J., Rovira, M., Martinez-Esparza, A. (2005) Radiolytic modelling of spent fuel oxidative dissolution mechanism. Calibration against UO_2 dynamic leaching experiments. J Nucl Mater 346, 40–47.

Millero, F.J., Sotolongo, S. (1989). The oxidation of Fe(II) with H_2O_2 in seawater. Geochim Cosmochim Acta 53, 1867–1873.

Neck, V., Kim, J.I. (2001). Solubility and hydrolysis of tetravalent actinides. Radiochim Acta 89, 1–16.

Nilsson, S., Jonsson, M., (2011). H_2O_2 and radiation induced dissolution of UO_2 and SIMFUEL pellets. J Nucl Mater 410, 89–93.

Odorowski, M., Jégou, C., De Windt, L., Broudic, V., Peuget, S., Magnin, M., Tribet, M., Martin, C. (2016). Oxidative dissolution of unirradiated Mimas MOX fuel (U/Pu oxides) in carbonate water under oxic and anoxic conditions. J Nucl Mater 468, 17–25.

Odorowski, M., Jegou, C., De Windt, L., Broudic, V., Jouan, G., Peuget, S., Martin, C. (2017). Effect of metallic iron on the oxidative dissolution of UO_2 doped with a radioactive alpha emitter. Geochim Cosmochim Acta 219, 1–21.

Pehrman, R., Trummer, M., Lousada, C.M., Jonsson, M. (2012). On the redox reactivity of doped UO_2 pellets – Influence of dopants on the H_2 O_2 decomposition mechanism. J Nucl Mater 430 (2012) 6–11.

Shoesmith, D.W. (2000) Fuel corrosion processes under waste disposal conditions. J Nucl Mater 282, 1–31.

Spahiu, K., Cui, D.Q., Lundstrom, M. (2004). The fate of radiolytic oxidants during spent fuel leaching in the presence of dissolved near field hydrogen. Radiochim Acta 92, 625–629.

Stroes-Gascoyne, S., Garisto, F., Betteridge, J.S. (2005). The effects of alpha-radiolysis on UO_2 dissolution determined from batch experiments with Pu-doped UO_2. J Nucl Mater 346, 5–15.

Ulrich, K.U., Singh, A., Schofield, E.J., Bargar, J.R., Veeramani, H., Sharp J.O., Bernier-Latmani, R., Giammar, D.E. (2008). Dissolution of biogenic and synthetic UO_2 under varied reducing conditions. Environ Sci Technol 42, 5600–5606.

van der Lee, J., De Windt, L., Lagneau, V., Goblet, P. (2003). Module-oriented modeling of reactive transport with HYTEC. Comput Geosci 29, 265–275.